Analytical model for calibrating laser intensity in strong-field-ionization experiments

Song-Feng Zhao, Anh-Thu Le, Cheng Jin, Xu Wang, and C. D. Lin

Phys. Rev. A **93**, 023413 — Published 11 February 2016

DOI: 10.1103/PhysRevA.93.023413

An analytical model for calibrating laser intensity in strong field ionization experiments

Song-Feng Zhao,[1,2] Anh-Thu Le,[1] Cheng Jin,[1,3] Xu Wang,[1] and C. D. Lin[1]

[1] *J. R. Macdonald Laboratory, Physics Department, Kansas State University, Manhattan, Kansas 66506-2604, USA*

[2] *College of Physics and Electronic Engineering, Northwest Normal University, Key Laboratory of Atomic and Molecular Physics and Functional Materials of Gansu Province, Lanzhou 730070, People's Republic of China*

[3] *School of Science, Nanjing University of Science and Technology, Nanjing, Jiangsu 210094, People's Republic of China*

The interaction of an intense laser pulse with atoms and molecules depends extremely nonlinearly with the laser intensity. Yet experimentally there still exists no simple reliable methods for determining the peak laser intensity within the focused volume. Here we present a simple method, based on an improved Perelomov-Popov-Terent'ev (PPT) model, that would allow the calibration of laser intensities from the measured ionization signals of atoms or molecules. The model is first examined by comparing ionization probabilities (or signals) of atoms and several simple diatomic molecules with those from solving the time-dependent Schrödinger equation. We then show the possibility of using this method to calibrate laser intensities for atoms, diatomic molecules as well as large polyatomic molecules, for laser intensities from the multiphoton ionization to tunneling ionization regimes.

PACS numbers: 33.80.Rv, 42.50.Hz

I. INTRODUCTION

When an atom or molecule is exposed to an intense laser field, a valence electron can be removed by absorbing several photons (so-called multiphoton ionization) [1, 2] or by tunneling through the potential barrier formed by the Coulomb force and the laser field (i.e.,tunnelling ionization) [3–6]. According to the Keldysh theory [7], these two ionization mechanisms can be distinguished by the Keldysh parameter $\gamma = \sqrt{I_p/2U_p}$, where I_p is the ionization potential and U_p is the quiver energy of the laser field. The multiphoton ionization dominates if $\gamma > 1$, while tunnelling ionization prevails when $\gamma < 1$. In a typical experiment, the laser beam is focused into a gas jet or a gas cell. It is desirable to know precisely the peak laser intensity at the focus. This peak intensity has been usually estimated from the $2U_p$ cutoff of low-energy electron spectra, or the $10U_p$ cutoff of high-energy electron spectra, as well as the cutoff $3.2U_p + I_p$ in the high-order harmonic spectra. In actual experiments, such cutoffs are usually not so clear because the signals are collected from a distributions of laser intensities within the focus volume, as well as other factors from the target structure. Furthermore, these cutoff energies are derived from the tunnel ionization model, thus they would become invalid toward the multiphoton ionization regime.

Experimentally, determination of ionization signals requires the least effort since only the cation yields have to be measured. If these yields are compared to ionization probabilities calculated using accurate theoretical methods, then intensity calibration in the experiment can be accomplished. Accurate calculations of ionization probability for a fixed laser intensity can be accomplished by solving the time-dependent Schrödinger equation (TDSE) for atoms and some small molecules [8–19], mostly based on the single-active-electron (SAE) model. Calculations including all electrons in the atom or molecules have been used within the time-dependent density functional theory (TDDFT) [20–25], the time-dependent Hatree-Fock (TDHF) theory [26, 27], or the multiconfiguration time-dependent Hatree-Fock (MCTDHF) theory [28–30]. These calculations are very time-consuming and their accuracy is also difficult to judge. It is not practical to perform such calculations to calibrate peak laser intensity in an experiment. Simpler ionization model like the ADK (Ammosov-Delone-Krainov) model [31] is reasonable accurate in the tunnel ionization regime, but its accuracy deteriorates quickly as laser intensity is decreased, or when the Keldysh parameter begins to become greater than 1.0. The ADK model has also been generalized to molecular targets (the MO-ADK) [32, 33, 35–39, 69] but it would again fail in the multiphoton ionization regime.

An alternative simple model for ionization is based on the first-order theory in a strong laser field, known as the Keldysh-Faisal-Reiss (KFR) [7, 40–43] theory. The KFR theory is known to be unable to correctly predict absolute ionization probability, yet it does predict fair intensity dependence. Over the years, beginning with the original PPT (Perelomov-Popov-Terent'ev) theory [44–46], various corrections have been introduced, and extended to molecules as well [10, 47–50]. We comment that there are other ionization theories, such as the nonadiabatic tunnelling ionization (NTI) [51] theory, the weak-field asymptotic theory (WFAT) [52–56] and so on. We will focus on the newer version of the PPT theory [47] which offers simplicity and proven accuracy. It also gives cycle-averaged ionization rates analytically.

In this work, we first evaluate the improved PPT model [47] which includes a more accurate Coulomb correction term. Our main goal here is to show that within a tolerable error this version of the PPT model can be efficiently and conveniently used by experimentalists to retrieve accurate peak laser intensity from measured ionization signals. The rest of this paper is arranged as follows. In Section 2, we first describe how we solved the single-electron TDSE for a model atom to obtain accurate total ionization probability. The results from such calculations will be served as "experimental" data to calibrate against results from the improved PPT theory [47] for a few targets and wavelengths. We will show that within reasonably acceptable errors, there is no need to rescale the ionization yields calculated from this improved PPT theory. In atoms we show that this improved PPT theory approaches the ADK theory at the tunnel ionization limit, thus we generalize this improved PPT theory to molecular targets by following the method of extending the ADK to the MO-ADK theory [50]. In Section 3, we demonstrate the typical remaining errors of the improved PPT model by comparing with the TDSE results and the experimental data. We then show how to calibrate laser intensity using ionization probability obtained from the PPT model, including ionization of polyatomic molecules. A conclusion will be given in Section 4. Atomic units are used throughout this paper unless otherwise stated.

II. THEORETICAL METHODS

The theory part is divided into two subsections. We first summarize how results are obtained from solving the TDSE for a model one-electron atom. We then present relevant basic equations of the improved PPT model [47] used in our calculations.

A. The method of solving TDSE for atoms in a laser field

Under the one-electron approximation and using the length gauge, the TDSE describing a one-electron atom in the presence of a linearly polarized laser field can be written as

$$i\frac{\partial}{\partial t}\psi(\mathbf{r},t) = [H_0(\mathbf{r}) + H_i(\mathbf{r},t)]\psi(\mathbf{r},t) \tag{1}$$

where $H_0(\mathbf{r})$ is the field-free Hamiltonian

$$H_0(\mathbf{r}) = -\frac{1}{2}\frac{d^2}{dr^2} + \frac{\hat{L}^2}{2r^2} + V(\mathbf{r}) \tag{2}$$

with $\hat{L}$ being the angular momentum operator. The single-electron atomic model potential $V(\mathbf{r})$ is parameterized as [57]

$$V(r) = -\frac{1+\beta(a_1e^{-a_2r} + a_3re^{-a_4r} + a_5e^{-a_6r})}{r} \tag{3}$$

For the He, Ne and Ar targets, all the parameters in Eq.(3) can be found in Ref. [57]. For Xe atom, a_1, a_2, a_3, a_4, a_5 and a_6 are taken to be 51.3555, 2.1116, -99.9275, 3.7372, 1.6445 and 0.4306, respectively. For Kr atom, we use the model potential proposed by Garvey *et al.* [58]. Note that $\beta = 1$ for real atoms or ions. The parameter β is introduced to adjust the ionization potential of a fictitious atom which would give a desired ionization potential. It modifies the potential close to the inner region of the atom only. Note that the Keldysh parameter depends only on the target ionization potential.

The electron-laser-field interaction $H_i(\mathbf{r},t)$ can be expressed as

$$H_i(\mathbf{r},t) = zF(t) \tag{4}$$

where $F(t)$ is the electric field of the laser pulse. Eq.(1) can be efficiently solved by using the time-dependent generalized pseudospectral method [59, 60]. In the present calculations, we use the following absorbing function

$$cos^{0.25}[\pi(r-r_0)/2(r_{max}-r_0)] \tag{5}$$

for r $\geq r_0$ and 1.0 elsewhere. The truncated radii are $r_{max} = 400a.u.$, $r_0 = 390a.u.$, the total spatial grid points, $N = 800$, time step, $dt = 0.1a.u.$, and up to 80 partial waves are used.

Once the time-dependent wavefunction is obtained, the total ionization probability of the atom at the end of the laser field is calculated from

$$P_{tot} = 1 - \sum_n |\langle\phi_n(\mathbf{r})|\psi(\mathbf{r},t_{final})\rangle|^2 \tag{6}$$

where n runs over all the bound states of the atom.

B. The PPT model

An improved PPT model with new recommended Coulomb correction has been given in [47] for atoms. The cycle-averaged ionization rate can be expressed as

$$\begin{aligned} w_{PPT}(F_0,\omega) &= (\frac{3F_0}{\pi\kappa^3})^{1/2}\frac{C_l^2}{2^{|m|}|m|!}\frac{(2l+1)(l+|m|)!}{2(l-|m|)!} \\ &\times \frac{A_m(\omega,\gamma)}{\kappa^{2Z_c/\kappa-1}}(1+\gamma^2)^{|m|/2+3/4} \\ &\times (\frac{2\kappa^3}{F_0})^{2Z_c/\kappa-|m|-1} \\ &\times (1+2e^{-1}\gamma)^{-2Z_c/\kappa} \\ &\times e^{[-(2\kappa^3/3F_0)g(\gamma)]} \end{aligned} \tag{7}$$

where C_l is the structure parameter of the atom, $e = 2.718...$, $\kappa = \sqrt{2I_p}$, and γ is the Keldysh parameter. Here, F_0, ω and Z_c are the laser's peak field strength, laser wave vector, and the asymptotic charge seen by the electron, respectively. In this equation, $g(\gamma)$ can be written as

$$g(\gamma) = \frac{3}{2\gamma}[(1+\frac{1}{2\gamma^2})sinh^{-1}\gamma - \frac{\sqrt{1+\gamma^2}}{2\gamma}] \tag{8}$$

and the coefficient $A_m(\omega,\gamma)$, which is more complex, can be found in Refs. [44, 48, 49]. In the limit of $\gamma \to 0$, $A_m(\omega,\gamma)$, $(1+\gamma^2)^{|m|/2+3/4}$, $g(\gamma)$ and $(1+2e^{-1}\gamma)^{-2Z_c/k}$ all go to 1.0 and the ADK model is recovered.

This PPT model can be extended to molecular targets, called MO-PPT [10, 50]. For completeness, the cycle-averaged ionization rate for a molecule fixed in space is expressed by

$$\begin{aligned} w_{MO-PPT}(F_0,\omega,\mathbf{R}) &= (\frac{3F_0}{\pi\kappa^3})^{1/2}\sum_{m'}\frac{B^2(m')}{2^{|m'|}|m'|!} \\ &\times \frac{A_{m'}(\omega,\gamma)}{\kappa^{2Z_c/\kappa-1}}(1+\gamma^2)^{|m'|/2+3/4} \\ &\times (\frac{2\kappa^3}{F_0})^{2Z_c/\kappa-|m'|-1} \\ &\times (1+2e^{-1}\gamma)^{-2Z_c/\kappa} \\ &\times e^{[-(2\kappa^3/3F_0)g(\gamma)]} \end{aligned} \quad (9)$$

For a linear molecule, $B(m')$ can be written as

$$B(m') = \sum_l C_{lm} D^l_{m',m}(\mathbf{R}) Q(l,m') \quad (10)$$

For a nonlinear molecule,

$$B(m') = \sum_{lm} C_{lm} D^l_{m',m}(\mathbf{R}) Q(l,m') \quad (11)$$

where the C_{lm} are structure parameters (i.e., expansion coefficients) of the molecule and $\mathbf{R}$ is the Euler angles of the molecular frame with respect to the laboratory fixed frame. $D^l_{m',m}(\mathbf{R})$ is the rotation matrix and

$$Q(l,m') = (-1)^{(m'+|m'|)/2}\sqrt{\frac{(2l+1)(l+|m'|)!}{2(l-|m'|)!}} \quad (12)$$

In this MO-PPT model, it reduces to the MO-ADK model [32] in the tunneling ionization limit. The two models use the same structure parameters.

Once the cycle-averaged ionization rates of molecules are obtained, we can calculate the total ionization probability by a laser pulse from

$$P(I,\mathbf{R}) = 1 - \exp(-\int_{-\infty}^{+\infty} w[F(t),\mathbf{R}]dt) \quad (13)$$

where $F(t)$ is the envelope of the laser pulse. If the molecules are randomly distributed, the alignment averaged total ionization probability is given by

$$P_{ave}(I) = \frac{1}{4\pi}\int_0^{2\pi}\int_0^{\pi} P(I,\mathbf{R}) sin\theta d\theta d\chi \quad (14)$$

To consider the volume effect of a focused laser pulse, the ionization signal of atoms or molecules has to be calculated as

$$S(I_0) \propto \int_0^{I_0} P(I)[-\frac{\partial V}{\partial I}]dI \quad (15)$$

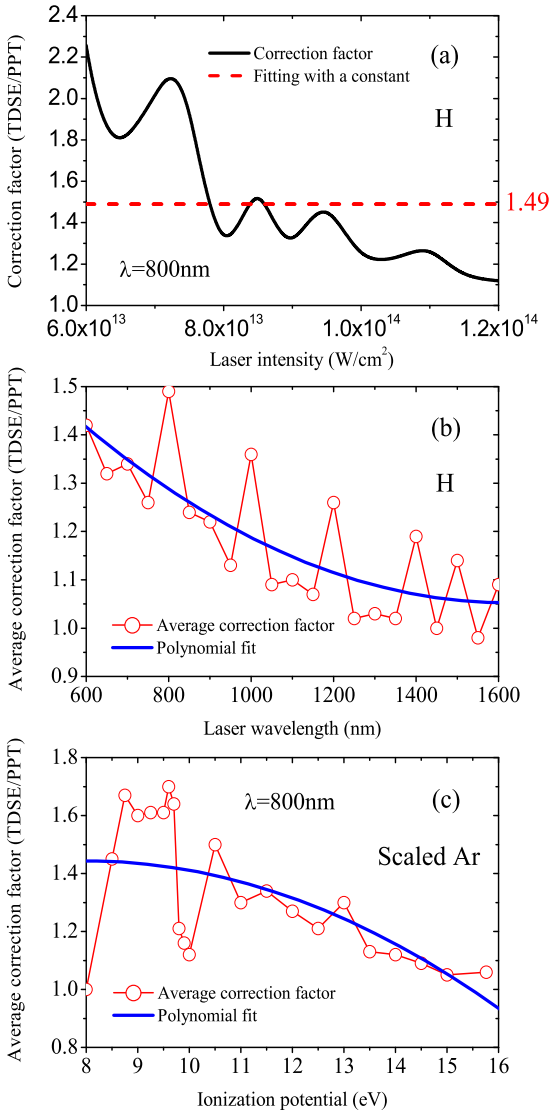

FIG. 1: (Color online) (a) The correction factor (TDSE/PPT) for the two cycle-averaged ionization probabilities of H atom versus laser intensity. The average of the correction factors is taken to be 1.49. (b) The average correction factor of H atom versus laser central wavelength; (c) The average correction factor of the scaled Ar atom versus ionization potential.

Here I_0 is the peak intensity at the focal point and the volume element takes the form $-\frac{dV}{dI} \propto (2I+I_0)(I_0-I)^{1/2}I^{-5/2}$ if we assume that the spatial distribution of the laser intensity is Gaussian.

III. RESULTS AND DISCUSSION

A. Calibration of PPT and MO-PPT models against TDSE results

The ionization rates (or probabilities) obtained from the PPT (or MO-PPT) for a given laser pulse is expected to differ from solving the TDSE. In Fig. 1(a) we show

the correction factor (i.e., TDSE/PPT) for 800 nm laser pulse on atomic hydrogen. The correction factor oscillates but is within about a factor of two over the intensity range shown. The oscillation is due to the ionization probability from the TDSE calculations [61]. For simplicity, we took the average correction factor to be 1.49 for 800 nm laser. We then check how this average correction factor changes with the wavelength of the laser. The results are shown in Fig. 1(b). Again the value oscillates with laser wavelength. By drawing a smooth curve again, the correction is between 1.1 and 1.4. We next used a fictitious Ar atom where the parameter β in Eq.(3) has been adjusted such that the ionization potential from 3p shell is ranging from 8 eV to 16 eV. The smoothed correction factor thus derived covers from 1.4 to 1.1. These two results indicate the correction factor typically is within about a factor of two. Since ionization by a strong intense laser field is highly nonlinear, a factor of two error in ionization rate would affect little the corresponding peak laser intensity. In the following we will test this assumption further.

We next compare the PPT and ADK models against TDSE calculations. Figure 2 shows ionization probabilities of H atom obtained from the TDSE, the PPT and the ADK methods at laser wavelengths of 600nm, 800nm, 1000nm and 1200nm, respectively. We can see that ionization probabilities from the PPT and TDSE agree very well, whether the correction factor for PPT is used or not. In contrast, the ADK theory fails drastically as the laser intensity is decreased, in the intensity region where the Keldysh parameter is greater than 1.0. The ADK model works well only for $\gamma < 1.0$. Clearly this shows that one should use the tunneling model carefully for calculating ionization probabilities. The PPT model, on the other hand, can be used over an extended laser intensity region. At the higher intensity where the ionization rate does not grow as rapidly with increasing intensity, as shown in the insets, the introduction of correction factors in PPT indeed improves the agreement with TDSE. Still, to read laser intensity from the PPT with and without correction factor would amount to only a few percents in the retrieved peak laser intensity.

In Fig. 3, we check ionization probabilities of five rare-gas atoms (i.e., He, Ne, Ar, Kr and Xe) obtained from the PPT model by comparing with those from the TDSE. The uncorrected PPT probabilities are in good agreement with those from the TDSE in general, while the ADK model fails quickly at lower intensity. In each figure, one can see that at γ=1.5, error from the ADK model is already by a factor of about 10. Figure 4 compares the ionization ratios of PPT/TDSE and of ADK/TDSE versus $1/\gamma$. Clearly the improvement of the PPT over ADK is drastic as the laser intensity is decreased. These ratios were taken from data shown in Fig. 3.

In Fig. 5 we compare the present ionization probabilities of the H_2 molecule for wavelengths of 800 nm, 400 nm and 266 nm, calculated from the MO-PPT and the MO-ADK models with those of SAE-TDSE, using

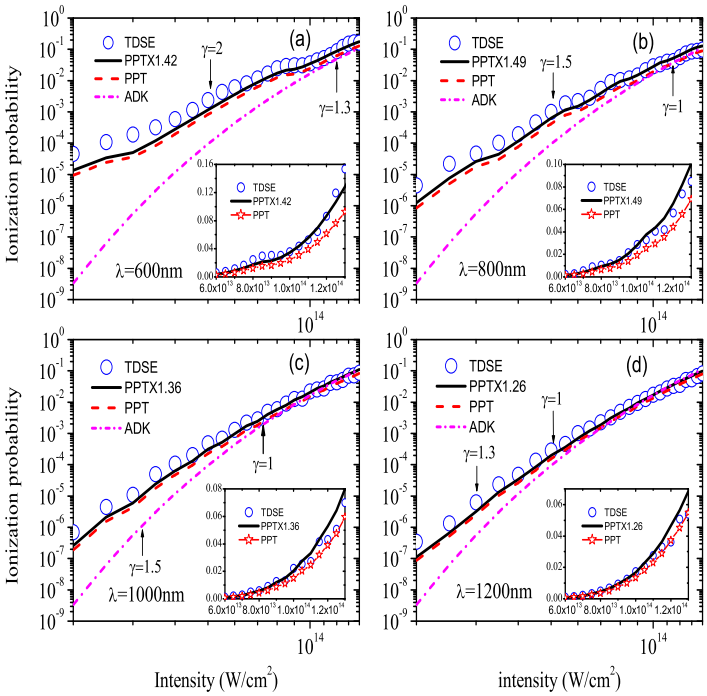

FIG. 2: (Color online) Comparison of ionization probabilities of H atom from the TDSE, the PPT and the ADK methods. (a) Wavelength $\lambda = 600nm$; (b) $\lambda = 800nm$; (c) $\lambda = 1000nm$; (d) $\lambda = 1200nm$. A Gaussian pulse with duration of 15 fs (full width at half maximum,FWHM) is used. Each inset zooms in the higher intensity region to reveal the error in probability.

the Hartree-Fock functionals [62]. We can see that ionization probabilities obtained from the MO-PPT model agree very well with those of the SAE-TDSE results in the whole range covering from the multiphoton to tunneling ionization regions, while the MO-ADK model works well only in the tunneling ionization region. From all of these examples, it is clear that ADK model fails to give accurate ionization probability generally when the Keldysh parameter becomes greater than 1.0.

In Fig. 6, we further check the PPT and the MO-PPT models by comparing ionization signals with experimental data [63] for Ar, Xe, N_2 and O_2. We mention that molecules are assumed to be randomly distributed in our simulations. Clearly both the PPT and the MO-PPT models fit reasonably well with the experimental data. Volume integration has been included in the calculations. It is interesting to point out that the ionization signals were calculated for a model one-electron atom while the targets for experimental data are real multi-electrons atoms or molecules. Based on the results in Fig. 6 one can state that strong field ionization is not severely modified by many-electron effect in general. We also note that in the multiphoton ionization regime the role of excited states may play a more important role in ionization. They are not included in the PPT model.

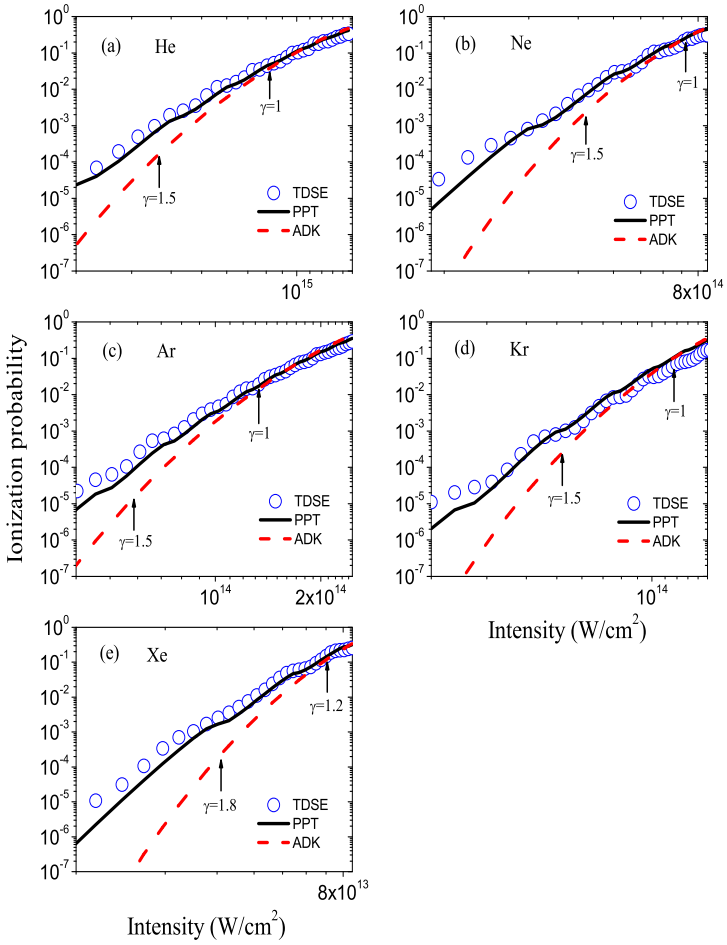

FIG. 3: (Color online) Comparison of ionization probabilities of rare-gas atoms from the TDSE, the PPT and the ADK methods. (a) He; (b) Ne; (c) Ar; (d) Kr; (e) Xe. The laser is taken to be a Gaussian pulse with FWHM of 15 fs. The central wavelength of the laser is 800 nm for Ar, Kr and Xe, and 400 nm for He and Ne.

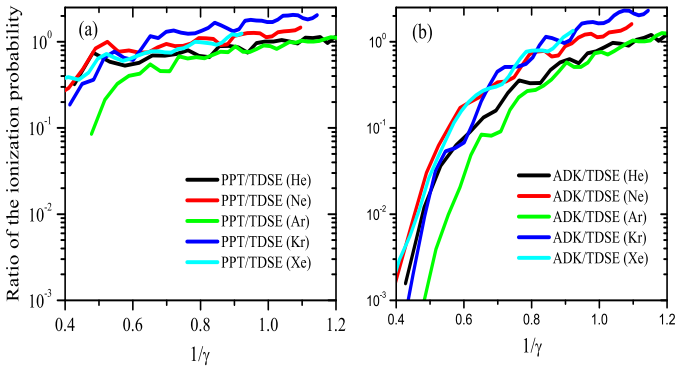

FIG. 4: (Color online) Comparison of ratios of ionization probabilities, (a) PPT/TDSE and (b) ADK/TDSE, versus the inverse of the Keldysh parameter, for rare-gas atoms. Data are the same as in Fig. 3.

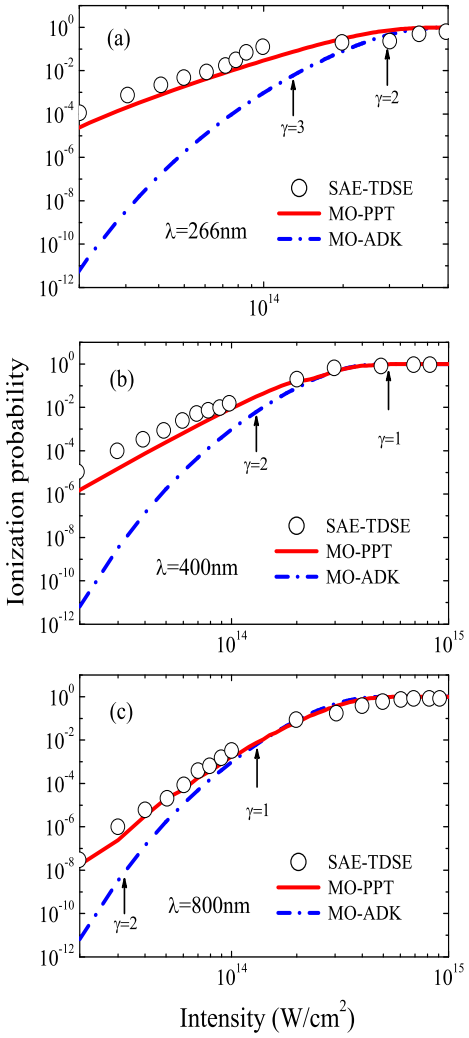

FIG. 5: (Color online) Comparison of ionization probabilities of the H_2 molecule from the SAE-TDSE [62], the MO-PPT and the MO-ADK methods at central wavelength of (a) 266 nm; (b) 400nm; (c) 800nm. The laser field is a cosine square pulse with 36 cycles, 24 cycles and 12 cycles, for 266 nm, 400 nm and 800 nm, respectively.

B. Strong field ionization of large polyatomic molecules

Strong field ionization so far has not been widely studied for large polyatomic molecules. Here we investigate several aromatic molecules that have been reported in the literature. Uiterwaal and his group [64–66] have reported ionization of several organic molecules in a micrometer-sized interaction volume and measured the time-of-flight in an ion mass spectrometer using 50 fs, 800 nm laser pulses. The novel feature of their setup is that it allows the measurement of ionization yields without the need to carry out volume integration. Aromatic molecules typically have low ionization energies, from about 8 to 10 eV. Thus their ionization by 800 nm lasers tends to have Keldysh parameters greater than 1.0, which is closer to the multiphoton ionization regime. Ab initio calculations

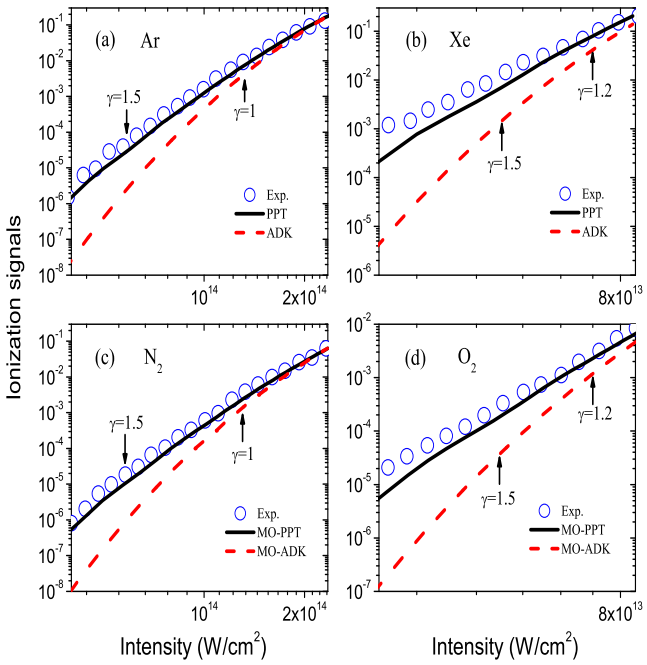

FIG. 6: (Color online) Comparison of ionization signals as a function of peak laser intensity. (a) Ar; (b) Xe; (c) N_2; (d) O_2. The laser field is a Gaussian pulse with central wavelength of 800nm and FWHM of 30fs. The experimental data are from Ref. [63].

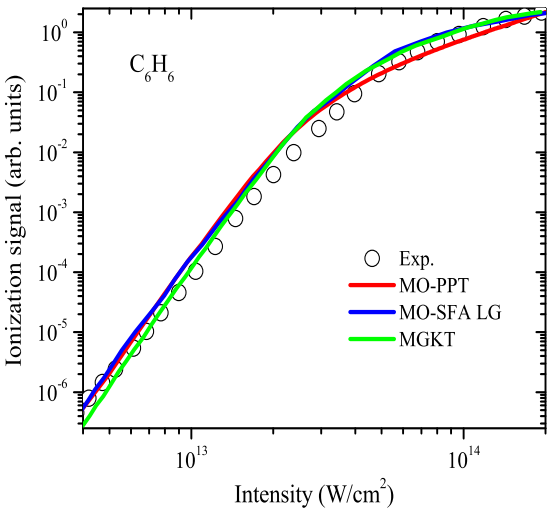

FIG. 7: (Color online) Comparison of experimental ionization signals of C_6H_6 vs MO-PPT model, as a function of laser intensity. The laser is a Gaussian pulse with wavelength of 800 nm and FWHM of 200 fs. The experimental data is from [67] and the two other model calculations are from Refs. [69, 70].

of strong field ionization for such large molecules are difficult. Here we apply the present version of the MO-PPT theory to these systems.

First, we consider the simplest aromatic molecule, the benzene, C_6H_6, which has ionization potential of 9.24 eV. Ionization of benzene without dissociation (by selecting $C_6H_6^+$ ions) has been reported earlier by Talebpour et.

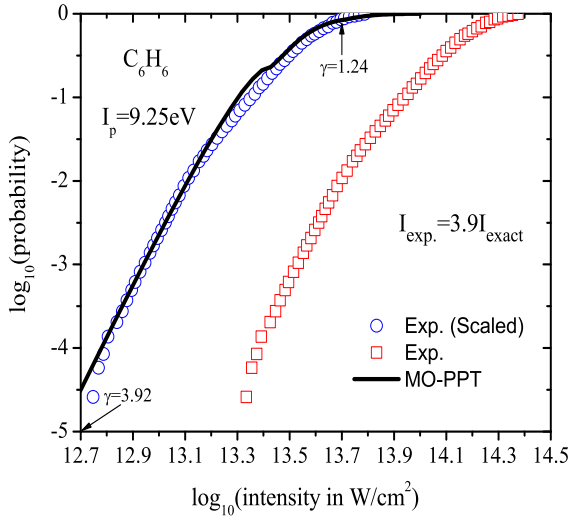

FIG. 8: (Color online) Ionization probabilities of C_6H_6 as a function of laser intensity. The laser is a Gaussian pulse with wavelength of 804 nm and FWHM of 50 fs. Experiment from Ref. [65]. Volume integration is not needed in the experimental data .

al. [67] using 200 fs, 800 nm laser pulses. Figure 7 shows their reported ionization yields, normalized to the ion yields calculated from the present molecular PPT theory at the intensity of 2×10^{14}W/cm^2. In the calculation, volume integration is included by assuming that the spatial intensity distribution is Gaussian and that the focal volume is smaller than the gas cell. Using the peak laser intensities in the experimental paper, we show that the present MO-PPT calculation agrees very well with their experimental data. In Fig. 7 we also show that the two other theories also gave good agreement with the experiment. Both of these theories are based on the multiphoton ionization models.

Next, we compare the results of the present molecular PPT model with the experimental data for benzene from [65], see Fig. 8. Taking the experimental intensities at their "face values" (Figure 1 of the cited paper) the ionization probability curve (normalized to 1.0 where the curve flattens out) is shown by the red squares in Fig.8, while the ionization probability calculated from MO-PPT theory is given by the black curve — at much lower intensities. If we reduce the experimental intensities by a factor of 3.91, as shown by blue circles, the experimental data would agree with the present MO-PPT calculations. We did find in Fig. 6 and the Appendix of [65] that "our data is shifted in intensity by a constant factor to compensate for differences in intensity calibration...". This shift factor was about 2.0. Nevertheless, by our new correction factor, the present MO-PPT theory would agree very well with the experimental data of [65].

Strong field ionization has also been reported in [65] for C_6H_5(F,Cl, Br, I) where one of the H atoms is replaced by F, Cl, Br and I, respectively. Figure 9 shows sketches of these molecules and their highest occupied

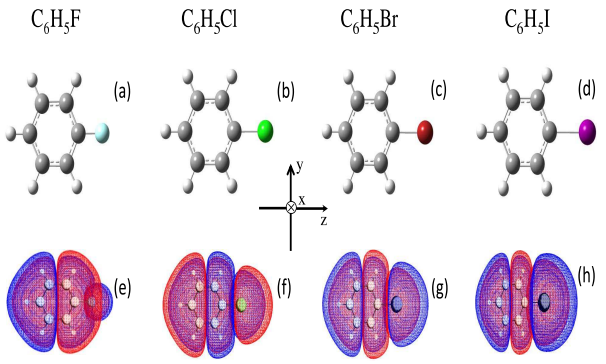

FIG. 9: (Color online) The first row gives atomic configurations of azabenzenes. The second row shows the iso-intensity contour plot of the highest occupied molecular orbital (HOMO).

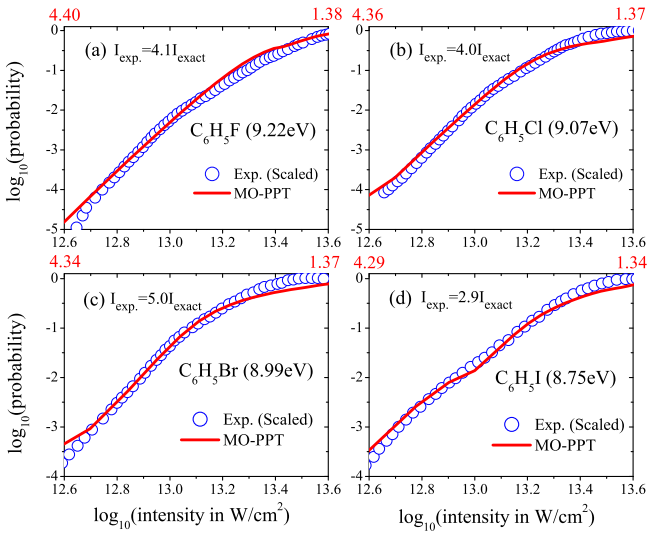

FIG. 10: (Color online) Ionization probabilities of azabenzenes as a function of laser intensity. The laser is a Gaussian pulse with wavelength of 804 nm and FWHM of 50 fs. Experimental data are taken from Ref. [65]. Keldysh parameters are presented on the top of each panel.

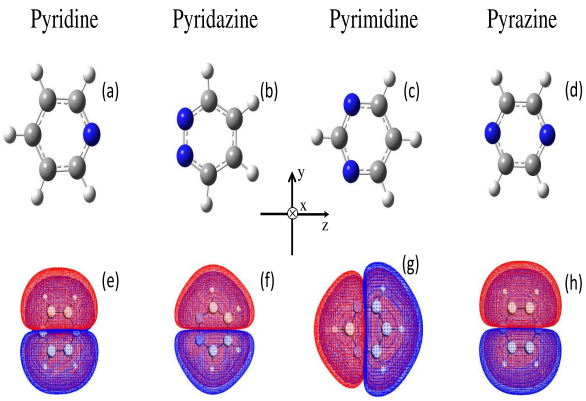

FIG. 11: (Color online) The first row gives atomic configurations of monohalobenzenes. The second row shows the iso-intensity contour plot of the HOMO for each molecule.

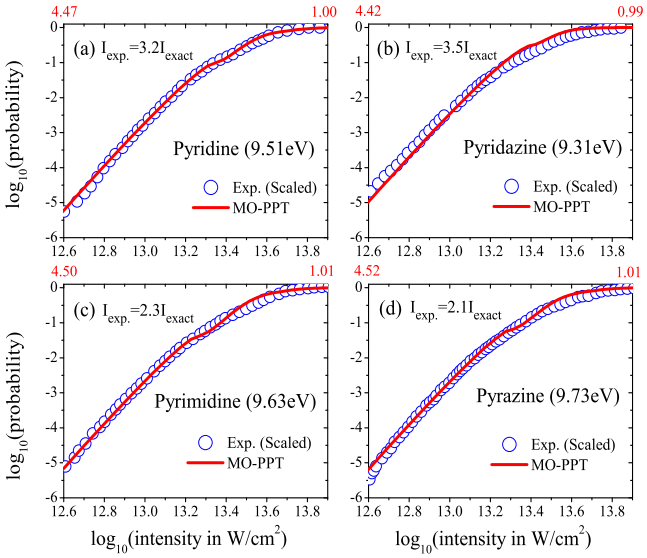

FIG. 12: (Color online) Ionization probabilities of monohalobenzenes as a function of laser intensity. The laser is a Gaussian pulse with wavelength of 800 nm and FWHM of 50 fs. Experimental data are from Ref. [66]. Keldysh parameters are given on the top of each panel.

molecular orbitals (HOMO). They do not differ too much. As the substituting atom becomes heavier, the ionization potential of the HOMO decreases. Figure 10 shows the reported experimental ionization signals, the normalized signal and the shift factors which have been adjusted such that they best fit MO-PPT simulations. The ionization potential and the corresponding range of Keldysh parameters are also shown in each figure. Overall, the agreement is very good. This confirms that indeed in the experiment of [65], the measured ionization probability does NOT require volume integration– a major feature of their experiments.

Finally we consider strong field ionization of pyridine, pyridazine, pyrimidine and pyrazine. These are benzene molecules where one or more pairs of the C-H arm is replaced by a single N atom. The geometry and the molecular orbital for each molecule are shown in Fig. 11 and they look very similar (molecules are not oriented in the experiment). Using the same normalization procedure, in Fig. 12 we show that the measured ionization curve agrees well with the one obtained from the MO-PPT theory. The ionization potential and the Keldysh parameters are also shown on each figure.

The structure parameters for these molecules have been calculated from molecular wavefunctions obtained from GAUSSIAN code [68]. These parameters and the x, y, z coordinates of each atom in these molecules are given in the Appendix.

Before closing this section, we do want to emphasize that comparison of ionization signal between theory and experiment for polyatomic molecules should al-

ways be taken with caution. In the theoretical calculations presented here, only ionization from the highest occupied molecular orbital (HOMO) is included. For some molecules, the binding energies of inner molecular orbitals (HOMO-1, HOMO-2, etc) can be quite close to the HOMO. Ionization from such orbitals may contribute directly to the ionization signals as well. For long pulses used in the experiment, rescattering from returning electrons also can contribute to the ionization signals. For more accurate comparison, the calculation should be compared to pure ionization, excluding signals from any molecular fragments.

IV. CONCLUSIONS

In this paper we examined the improved PPT model [47] for studying strong-field ionization of atoms and molecules. The model was tested carefully by comparing ionization probabilities of the H atom, rare-gas atoms and the H_2 molecule with those from the TDSE calculation. By including volume integration of the laser pulse, the PPT model is further checked by comparing with experimental ionization signals. We found that the PPT model can fit well the single-electron TDSE results and the experimental data over a broad range of laser intensities from the typical multiphoton regime to the tunneling ionization regime without the need of introducing a normalization factor. Using the molecular PPT model, we also demonstrated that it is possible to calibrate laser intensities in an experiment by measuring ionization signals over a range of laser intensities. This method is more accurate than other estimates based on the $2U_p$ cutoff of low-energy electrons or the $10U_p$ cutoff of high-energy electrons. In this work we also demonstrated that the ADK model works well only in the tunneling ionization region. Its prediction deteriorates quickly as the Keldysh parameter becomes larger than 1.0, see Fig. 4. The present PPT model, while a little bit more complicated to calculate than the simple ADK or the MO-ADK theories, is still quite simple because it is in analytical form. This work proved that this PPT model is quite adequate for a broad range of Keldysh parameters where strong field ionization probability is significant (say higher than 10^{-6}). Thus we recommend that the present PPT model be used to replace the ADK model for estimating ionization rate or probability for strong field ionization of atoms and molecules, and the present method be used to estimate peak laser intensities in experiments.

It is to be noted that the present ADK and PPT models for ionization are based on the dipole approximation. Recently it has been suggested that nondipole effect may play a role in strong field ionization [71]. While such effect has been studied recently [72, 73] showing small shift in the photoelectron momentum distributions in the propagation direction (less than 0.025 atomic units in momentum) for ionization of atoms by 3.4 μm laser at intensity of about 10^{14}W/cm^2 or lower, due to the presence of Lorentz force when nondipole effect is included, such small shift has no direct consequence on the total ionization probability which is the concern of this article. The main challenge in strong field experiments is the characterization of laser intensity and its distribution within the focused volume. For this purpose, any effect that modifies ionization of less than a few percent is not important, especially if we are to use the ionization yield to calibrate the intensity of the laser pulse.

Acknowledgments

This research was supported in part by Chemical Sciences, Geosciences and Biosciences Division, Office of Basic Energy Sciences,Office of Science, U. S. Department of Energy, and by National Science Foundation under Award No. IIA-1430493. S.-F.Z was also supported by the National Natural Science Foundation of China under Grant Nos. 11164025, 11264036, 11465016, 11364038, the Specialized Research Fund for the Doctoral Program of Higher Education of China under Grant No. 20116203120001 and the basic scientific research foundation for institution of higher learning of Gansu Province. We also thank Cornelis Uiterwaal for useful discussions on ionization from polyatomic molecules.

Appendix

[1] N. B. Delone, Sov. Phys. Usp. 18, 169 (1975).
[2] G. Mainfray and C. Manus, Rep. Prog. Phys. 54, 1333 (1991).
[3] V. P. Krainov, W. Xiong, and S. L. Chin, Laser Phys. 2, 467 (1992).
[4] N. B. Delone and V. P. Krainov, Phys. Usp. 41, 469 (1998).
[5] V. S. Popov, Phys. Usp. 47, 855 (2004).
[6] S. H. Lin, A. A. Villaeys, and Y. Fujimura, Advances in Multi-photon Processesand Spectroscopy, vol.16, World Scientific Publishing Co. Pte. Ltd, Singapore, 2004.
[7] L. V. Keldysh, Sov. Phys. JETP 20, 1307 (1965).
[8] J. L. Krause, K. J. Schafer, and K. C. Kulander, Phys. Rev. A 45, 4998 (1992).
[9] D. Bauer and P. Mulser, Phys. Rev. A 59, 569 (1999).
[10] S. -F. Zhao, L. Liu, and X. X. Zhou, Opt. Commun. 313, 74 (2014).
[11] A. Scrinzi, M. Geissler, and T. Brabec, Phys. Rev. Lett. 83, 706 (1999).
[12] S. Petretti, Y. V. Vanne, A. Saenz, A. Castro, and P.

Decleva, Phys. Rev. Lett. 104, 223001 (2010).
[13] M. Spanner and S. Patchkovskii, Phys. Rev. A 80, 063411 (2009).
[14] M. Abu-samha and L. B. Madsen, Phys. Rev. A 80, 023401 (2009).
[15] G. Lagmago Kamta and A. D. Bandrauk, Phys. Rev. A 74, 033415 (2006).
[16] Y. J. Jin, X. M. Tong, and N. Toshima, Phys. Rev. A 83, 063409 (2011).
[17] B. Zhang, J. Yuan, and Z. X. Zhao, Phys. Rev. A 85, 033421 (2012).
[18] S. Petretti, A. Saenz, A. Castro, and P. Decleva, Chem. Phys. 414, 45 (2013).
[19] S. L. Hu, Z. X. Zhao, and T. Y. Shi, Chin. Phys. Lett. 30, 103103 (2013).
[20] X. M. Tong and Shih-I.Chu, Phys. Rev. A 64, 013417 (2001).
[21] S. K. Son and Shih-I Chu, Phys. Rev. A 80, 011403 (R) (2009).
[22] D. A. Telnov and Shih-I Chu, Phys. Rev. A 79, 041401 (R) (2009).
[23] X. Chu, Phys. Rev. A 82, 023407 (2010).
[24] X. Chu and M. McIntyre, Phys. Rev. A 83, 013409 (2011).
[25] T. Otobe and K. Yabana, Phys. Rev. A 75, 062507 (2007).
[26] K. C. Kulander, Phys. Rev. A 36, 2726 (1987).
[27] B. Zhang, J. Yuan, and Z. X. Zhao, Phys. Rev. Lett. 111, 163001 (2013).
[28] D. J. Haxton, K. V. Lawler, and C. W. McCurdy, Phys. Rev. A 83, 063416 (2011).
[29] D. Hochstuhl and M. Bonitz, J. Chem. Phys. 134, 084106 (2011).
[30] J. Caillat, J. Zanghellini, M. Kitzler, O. Koch, W. Kreuzer, and A. Scrinzi, Phys. Rev. A 71, 012712 (2005).
[31] M. V. Ammosov, N. B. Delone, and V. P. Krainov, Sov. Phys. JETP 64, 1191 (1986).
[32] X. M. Tong, Z. X. Zhao, and C. D. Lin, Phys. Rev. A 66, 033402 (2002).
[33] Z. X. Zhao, X. M. Tong, and C. D. Lin, Phys. Rev. A 67, 043404 (2003).
[34] T. K. Kjeldsen and L. B. Madsen, Phys. Rev. A 71, 023411 (2005).
[35] S. -F. Zhao, C. Jin, A. -T. Le, T. F. Jiang, and C. D. Lin, Phys. Rev. A 80, 051402(R) (2009).
[36] S. -F. Zhao, C. Jin, A. -T. Le, T. F. Jiang, and C. D. Lin, Phys. Rev. A 81, 033423 (2010).
[37] S. -F. Zhao, C. Jin, A. -T. Le, and C. D. Lin, Phys. Rev. A 82, 035402 (2010).
[38] S. -F. Zhao, J. Xu, C. Jin, A. -T. Le, and C. D. Lin, J. Phys. B 44, 035601 (2011).
[39] J. P. Wang, S. -F. Zhao, C. R. Zhang, W. Li, and X. X. Zhou, Mol. Phys. 112, 1102 (2014).
[40] F. H. M. Faisal, J. Phys. B 6, L89 (1973).
[41] H. R. Reiss, Phys. Rev. A 22, 1786 (1980).
[42] J. Muth-Böhm, A. Becker, and F. H. M. Faisal, Phys. Rev. Lett. 85, 2280 (2000).
[43] T. K. Kjeldsen and L. B. Madsen, J. Phys. B 37, 2033 (2004).
[44] A. M. Perelomov,V. S. Popov, and M. V. Terent'ev, Sov. Phys. JETP 23, 924 (1966).
[45] A. M. Perelomov,V. S. Popov, and M. V. Terent'ev, Sov. Phys. JETP 24, 207 (1967).
[46] A. M. Perelomov and V. S. Popov, Sov. Phys. JETP 25, 336 (1967).
[47] S. V. Popruzhenko, V. D. Mur, V. S. Popov, and D. Bauer, Phys. Rev. Lett. 101, 193003 (2008).
[48] F. A. Ilkov, J. E. Decker, and S. L. Chin, J. Phys. B 25, 4005 (1992).
[49] Y. Z. Fu, S. -F. Zhao, and X. X. Zhou, Chin. Phys. B 21, 113101 (2012).
[50] E. P. Benis, J. F. Xia, X. M. Tong, M. Faheem, M. Zamkov, B. Shan, P. Richard, and Z. Chang, Phys. Rev. A 70, 025401 (2004).
[51] G. L. Yudin and M. Y. Ivanov, Phys. Rev. A 64, 013409 (2001).
[52] O. I. Tolstikhin, T. Morishita, and L. B. Madsen, Phys. Rev. A 84, 053423 (2011).
[53] L. B. Madsen, O. I. Tolstikhin, and T. Morishita, Phys. Rev. A 85, 053404 (2012).
[54] L. B. Madsen, F. Jensen, O. I. Tolstikhin, and T. Morishita, Phys. Rev. A 87, 013406 (2013).
[55] V. H. Trinh, O. I. Tolstikhin, L. B. Madsen, and T. Morishita, Phys. Rev. A 87, 043426 (2013).
[56] R. Saito, O. I. Tolstikhin, L. B. Madsen, and T. Morishita, Atomic data and Nuclear Data Tables 103-104,4 (2015).
[57] X. M. Tong and C. D. Lin, J. Phys. B 38, 2593 (2005).
[58] R. H. Garvey, C. H. Jackman, and A. E. S. Green, Phys. Rev. A 12, 1144 (1975).
[59] X. M. Tong and Shih-I Chu, Chem. Phys. 217, 119 (1997).
[60] S. -F. Zhao, X. X. Zhou, P. C. Li, and Z. Chen, Phys. Rev. A 78, 063404 (2008).
[61] Q. Li, X. M. Tong, T. Morishita, H. Wei, and C. D. Lin, Phys. Rev. A 89, 023421 (2014).
[62] M. Awasthi, Y. V. Vanne, A. Saenz, A. Castro, and P. Decleva, Phys. Rev. A 77, 063403 (2008).
[63] C. Guo, M. Li, J. P. Nibager, and G. N. Gibson, Phys. Rev. A 58, R4271 (1998).
[64] J. Strohaber and C. J. G. J. Uiterwaal, Phys. Rev. Lett. 100, 023002 (2008).
[65] T. D. Scarborough, J. Strohaber, D. B. Foote, C. J. McAcy, and C. J. G. J. Uiterwaal, Phys. Chem. Chem. Phys. 13, 13783 (2011).
[66] T. D. Scarborough, D. B. Foote, and C. J. G. J. Uiterwaal, J. Chem. Phys 136, 054309 (2012).
[67] A. Talebpour, A. D. Bandrauk, K. Vijayalakshmi, and S. L. Chin, J. Phys. B 33, 4615 (2000).
[68] M. J. Frisch, G. W. Trucks, H. B. Schlegel, G. E. Scuseria *et al.*, GAUSSIAN 03, Revision C.02 (Gaussian Inc. Pittsburgh, PA, 2003).
[69] T. K. Kjeldsen, C. Z. Bisgaard, L. B. Madsen, and H. Stapelfeldt, Phys. Rev. A 71, 013418 (2005).
[70] K. Nagaya, K. Mishima, H. -F. Lu, M. Hayashi, and S. H. Lin, Chem. Phys. Lett. 424, 34 (2006).
[71] H. R. Reiss, J. Phys. B 47, 204006 (2014).
[72] S. Chelkowski, A. D. Bandrauk, and P. B. Corkum, Phys. Rev. A 92, 051401(R) (2015).
[73] A. Ludwig, J. Maurer, B. W. Mayer, C. R. Phillips, L. Gallmann, and U. Keller, Phys. Rev. Lett. 113, 243001 (2014).

TABLE I: Fitted C_{lm} structure coefficients for several monohalobenzenes and azabenzenes. The experimental vertical ionization energies are also listed.

Molecule	Orbitals	I_p(eV)	C_{lm}							
C_6H_5F	$3b_1$(HOMO)	9.22	$C_{1\pm1}$	$C_{2\pm1}$	$C_{3\pm3}$	$C_{3\pm1}$	$C_{4\pm3}$	$C_{4\pm1}$	$C_{5\pm3}$	$C_{5\pm1}$
			∓0.44	±1.56	±0.06	∓0.96	∓0.17	±0.34	±0.07	∓0.27
C_6H_5Cl	$4b_1$(HOMO)	9.07	$C_{1\pm1}$	$C_{2\pm1}$	$C_{3\pm3}$	$C_{3\pm1}$	$C_{4\pm3}$	$C_{4\pm1}$	$C_{5\pm3}$	$C_{5\pm1}$
			±1.21	∓1.07	∓0.08	±2.18	±0.25	∓0.18	∓0.18	±0.95
C_6H_5Br	$6b_1$(HOMO)	8.99	$C_{1\pm1}$	$C_{2\pm1}$	$C_{3\pm3}$	$C_{3\pm1}$	$C_{4\pm3}$	$C_{4\pm1}$	$C_{5\pm3}$	$C_{5\pm1}$
			∓1.99	±1.54	±0.09	∓3.36	∓0.24	±1.48	±0.27	∓1.76
C_6H_5I	$8b_1$(HOMO)	8.75	$C_{1\pm1}$	$C_{2\pm1}$	$C_{3\pm3}$	$C_{3\pm1}$	$C_{4\pm3}$	$C_{4\pm1}$	$C_{5\pm3}$	$C_{5\pm1}$
			±0.64	∓1.07	∓0.17	±1.16	±0.16	∓0.37	∓0.12	±0.82
Pyridine	$1a_2$(HOMO)	9.51	$C_{2\pm2}$	$C_{4\pm4}$	$C_{4\pm2}$	$C_{6\pm6}$	$C_{6\pm4}$	$C_{6\pm2}$		
			∓1.63i	±0.37i	∓0.15i	∓0.03i	±0.04i	±0.02i		
Pyridazine	$1a_2$(HOMO)	9.31	$C_{2\pm2}$	$C_{4\pm4}$	$C_{4\pm2}$	$C_{6\pm6}$	$C_{6\pm4}$	$C_{6\pm2}$		
			±1.81i	∓0.27i	±0.48i	±0.03i	∓0.02i	±0.06i		
Pyrimidine	$2b_1$(HOMO)	9.63	$C_{2\pm1}$	$C_{4\pm3}$	$C_{4\pm1}$	$C_{6\pm5}$	$C_{6\pm1}$			
			∓2.10	±0.30	∓0.40	∓0.04	∓0.06			
Pyrazine	$1b_{1g}$(HOMO)	9.73	$C_{2\pm2}$	$C_{4\pm4}$	$C_{4\pm2}$	$C_{6\pm6}$	$C_{6\pm4}$	$C_{6\pm2}$		
			∓1.89i	±0.41i	∓0.17i	∓0.03i	±0.05i	±0.02i		

TABLE II: The x, y, z coordinates (in Angstroms) of atoms for several monohalobenzenes and azabenzenes at equilibrium calculated from the GAUSSIAN packages.

Molecule	atoms	x	y	z	Molecule	atoms	x	y	z
C_6H_5F	F	0.000000	0.000000	2.289972	C_6H_5Cl	Cl	0.000000	0.000000	2.267562
	C	0.000000	0.000000	0.927884		C	0.000000	0.000000	0.503122
	C	0.000000	1.220741	0.261313		C	0.000000	1.218591	-0.177764
	C	0.000000	-1.220741	0.261313		C	0.000000	-1.218591	-0.177764
	C	0.000000	1.210650	-1.137673		C	0.000000	1.209466	-1.576463
	C	0.000000	-1.210650	-1.137673		C	0.000000	-1.209466	-1.576463
	C	0.000000	0.000000	-1.838690		C	0.000000	0.000000	-2.278215
	H	0.000000	2.149699	0.829767		H	0.000000	2.155136	0.377292
	H	0.000000	-2.149699	0.829767		H	0.000000	-2.155136	0.377292
	H	0.000000	2.156666	-1.679794		H	0.000000	2.156766	-2.116783
	H	0.000000	-2.156666	-1.679794		H	0.000000	-2.156766	-2.116783
	H	0.000000	0.000000	-2.928531		H	0.000000	0.000000	-3.368302
C_6H_5Br	Br	0.000000	0.000000	1.814687	C_6H_5I	I	0.000000	0.000000	1.572114
	C	0.000000	0.000000	-0.104726		C	0.000000	0.000000	-0.582517
	C	0.000000	1.218417	-0.786483		C	0.000000	1.212010	-1.271446
	C	0.000000	-1.218417	-0.786483		C	0.000000	-1.212010	-1.271446
	C	0.000000	1.209495	-2.185422		C	0.000000	1.207411	-2.669013
	C	0.000000	-1.209495	-2.185422		C	0.000000	-1.207411	-2.669013
	C	0.000000	0.000000	-2.887206		C	0.000000	0.000000	-3.369919
	H	0.000000	2.157913	-0.236139		H	0.000000	2.148784	-0.729866
	H	0.000000	-2.157913	-0.236139		H	0.000000	-2.148784	-0.729866
	H	0.000000	2.157160	-2.725013		H	0.000000	2.149776	-3.204434
	H	0.000000	-2.157160	-2.725013		H	0.000000	-2.149776	-3.204434
	H	0.000000	0.000000	-3.977289		H	0.000000	0.000000	-4.453300
Pyridine (azabenzene)	N	0.000000	0.000000	1.421213	Pyridazine (1,2-diazine)	C	0.000000	0.693023	1.181141
	C	0.000000	0.000000	-1.387666		C	0.000000	-0.693023	1.181141
	C	0.000000	1.144618	0.723930		C	0.000000	-1.325661	-0.068077
	C	0.000000	-1.144618	0.723930		C	0.000000	1.325661	-0.068077
	C	0.000000	1.199948	-0.673661		H	0.000000	1.275944	2.102422
	C	0.000000	-1.199948	-0.673661		H	0.000000	-1.275944	2.102422
	H	0.000000	0.000000	-2.478549		H	0.000000	-2.413812	-0.153581
	H	0.000000	2.066084	1.311431		H	0.000000	2.413812	-0.153581
	H	0.000000	-2.066084	1.311431		N	0.000000	0.666906	-1.232460
	H	0.000000	2.162804	-1.185018		N	0.000000	-0.666906	-1.232460
	H	0.000000	-2.162804	-1.185018					
Pyrimidine (1,3-diazine)	C	0.000000	0.000000	1.356679	Pyrazine (1,4-diazine)	N	0.000000	0.000000	1.409020
	C	0.000000	0.000000	-1.312620		N	0.000000	0.000000	-1.409020
	C	0.000000	1.187029	0.623294		C	0.000000	1.134568	0.699700
	C	0.000000	-1.187029	0.623294		C	0.000000	-1.134568	0.699700
	N	0.000000	1.198653	-0.716332		C	0.000000	-1.134568	-0.699700
	N	0.000000	-1.198653	-0.716332		C	0.000000	1.134568	-0.699700
	H	0.000000	0.000000	2.446229		H	0.000000	2.073205	1.258453
	H	0.000000	0.000000	-2.404261		H	0.000000	-2.073205	1.258453
	H	0.000000	2.159814	1.121396		H	0.000000	-2.073205	-1.258453
	H	0.000000	-2.159814	1.121396		H	0.000000	2.073205	-1.258453